A Ca-Mg Synergistic Agonist for Trade-off CD8 T Cell Immunomodulation to Enhance Solid Tumor Immunotherapy

Jing Zhao[1], Aining Shen[1], Yu Wang[1], Boyi Li[1], Jinling Huang[1], Ying Li[1], Chun Xu[2,3], Zhi Ping Xu[1*], Lingxiao Zhang[2,3*]*

[1] Institute of Chemical Biology, Shenzhen Bay Laboratory, Shenzhen 518107, China.

[2] Faculty of Medicine and Health, The University of Sydney, Camperdown, New South Wales 2006, Australia

[3] Charles Perkins Centre, The University of Sydney, Camperdown, New South Wales 2006, Australia

Corresponding authors:

Lingxiao Zhang, E-mail: zhanglx@inano.au.dk

Zhi Ping Xu, E-mail: gordonxu@szbl.ac.cn

Chun Xu, E-mail: chun.xu@sydney.edu.au

Keywords: nano-aluminum adjuvant, $CD8^+$ T cell agonist, adoptive cell therapy, T cell exhaustion, cancer immunotherapy

Abstract

Adjuvants have traditionally been developed to activate antigen-presenting cells and thereby initiate adaptive immunity. Emerging evidence, however, indicates that adjuvants can also directly regulate T lymphocyte function. Here, we report a calcium-magnesium nano-aluminum adjuvant (CMA) that functions as a self-braking $CD8^+$ T cell agonist. By integrating complementary immunoregulatory activities of Ca^{2+} and Mg^{2+} within nano-aluminum platform, CMA dynamically modulates $CD8^+$ T cell activation and exhaustion to enhance the effector function. Following efficient cellular internalization, CMA enhances $CD8^+$ T cell activity under both physiological and lactic acid (LA)-rich conditions that mimic the tumor microenvironment. Mechanistically, CMA promotes oxidative phosphorylation and activates NFAT2 signaling to increase production of effector molecules, including interferon-γ and granzyme B. Concurrently, CMA suppresses AKT phosphorylation, preserves proteostasis, and attenuates the expression of exhaustion-associated inhibitory receptors. As a result, ex vivo CMA pretreatment endows $CD8^+$ T cells with sustained functionality and resistance to LA-mediated immunosuppression, leading to improved antitumor efficacy following adoptive cell transfer. In parallel, local administration of CMA directly activates tumor-resident $CD8^+$ T cells and suppresses tumor growth. Combining adoptive transfer of CMA-primed $CD8^+$ T cells with peritumoral CMA administration produces superior therapeutic efficacy against solid tumors. Collectively, this work establishes a biomaterial-based strategy for direct $CD8^+$ T cell regulation and highlights nano-engineered adjuvants as a versatile platform for enhancing cancer immunotherapy through dynamic control of T cell activation and exhaustion.

1. Introduction

$CD8^+$ T cells are central mediators of antitumor immunity against solid tumors, yet their efficacy is frequently constrained by progressive functional impairment within the tumor microenvironment (TME) [1]. Clinical strategies for enhancing $CD8^+$ T cell activity mainly rely on co-stimulatory antibodies and cytokines to induce receptor-mediated T-cell activation [2-3]. Although these approaches promote T-cell expansion and effector differentiation, persistent stimulation combined with the suppressive TME frequently drives T cell exhaustion, thereby limiting therapeutic durability [4-5]. Current strategies to mitigate exhaustion mainly include immune checkpoint blockade [6], metabolic reprogramming [7], and inhibiting pathways with small molecules such as AKT [8]. However, approaches capable of simultaneously enhancing effector activation while preventing hyperactivation-induced exhaustion remain limited.

Nutritional metal ions are essential for $CD8^+$ T cell activation and effector functions [9-10], while also governing cellular metabolic states by influencing ATP stability and the activity of multiple metabolic enzymes [11]. Amongst, calcium ion (Ca^{2+}) acts as a central second messenger that enhances the expression of nuclear factor of activated T cells (NFAT), thereby amplifying $CD8^+$ T cell activation and effector cytokine production [12-13]. Elevated cytoplasmic Ca^{2+} levels favor the metabolic routing of lactic acid (LA), promoting its mitochondrial metabolism [11]. However, excessive Ca^{2+} stimulation readily induces $CD8^+$ T cell exhaustion [14]. Complementarily, our recent work reveals that magnesium ion (Mg^{2+}) is essential for limiting T cell exhaustion [15], although the underlying mechanisms remain unclear. Apart from this function, Mg^{2+} also serves as a $CD8^+$ T cell agonist by promoting the conversion of surface leukocyte function-associated antigen I to an active state, enhancing immunological synapse formation and optimizing Ca^{2+} signaling efficiency [16]. Moreover, Mg^{2+} serves as an indispensable cofactor for ATP stabilization and multiple enzymatic reactions involved in cellular metabolism [17]. Therefore, we hypothesized that concurrent supplementation with Ca^{2+} and Mg^{2+} would enhance $CD8^+$ T cell effector function but limit exhaustion. Mg-based nano-aluminum adjuvant (MA) with its readily tunable metal ion composition holds great potential as a tailorable ion carrier [18]. Upon cellular uptake, MA undergoes lysosomal degradation, leading to the release of its constituent ions for immunomodulation. Besides, alkaline MA persistently neutralizes the acidic TME for over 2 weeks, thereby reversing the immunosuppressive TME and enhancing T cell infiltration [19-21]. Based on these properties, we

further hypothesized that MA supplemented with Ca^{2+} would be an efficient self-braking $CD8^+$ T-cell agonist capable of coordinately enhancing effector function while restraining exhaustion.

In this study, we designed a Ca-incorporated MA (CMA) adjuvant, delivering both Ca^{2+} and Mg^{2+} to enhance $CD8^+$ T cell effector function and mitigate exhaustion via Ca^{2+}-Mg^{2+} coordinated modulation. Ex vivo pretreatment of $CD8^+$ T cells with CMA followed by retro-orbital injection significantly promoted the therapeutic efficacy of adoptive T cell therapy, while peritumoral injection of CMA enhances the in-situ effector function of $CD8^+$ T cells. Mechanistically, CMA promotes oxidative phosphorylation (OXPHOS) and activates NFAT2 to enhance effector function, while inhibiting AKT phosphorylation (pAKT) to maintain proteostasis and reduce exhaustion. Moreover, CMA confers resistance to LA -mediated suppression, thereby preserving $CD8^+$ T-cell function under TME-mimicking conditions (Figure 1).

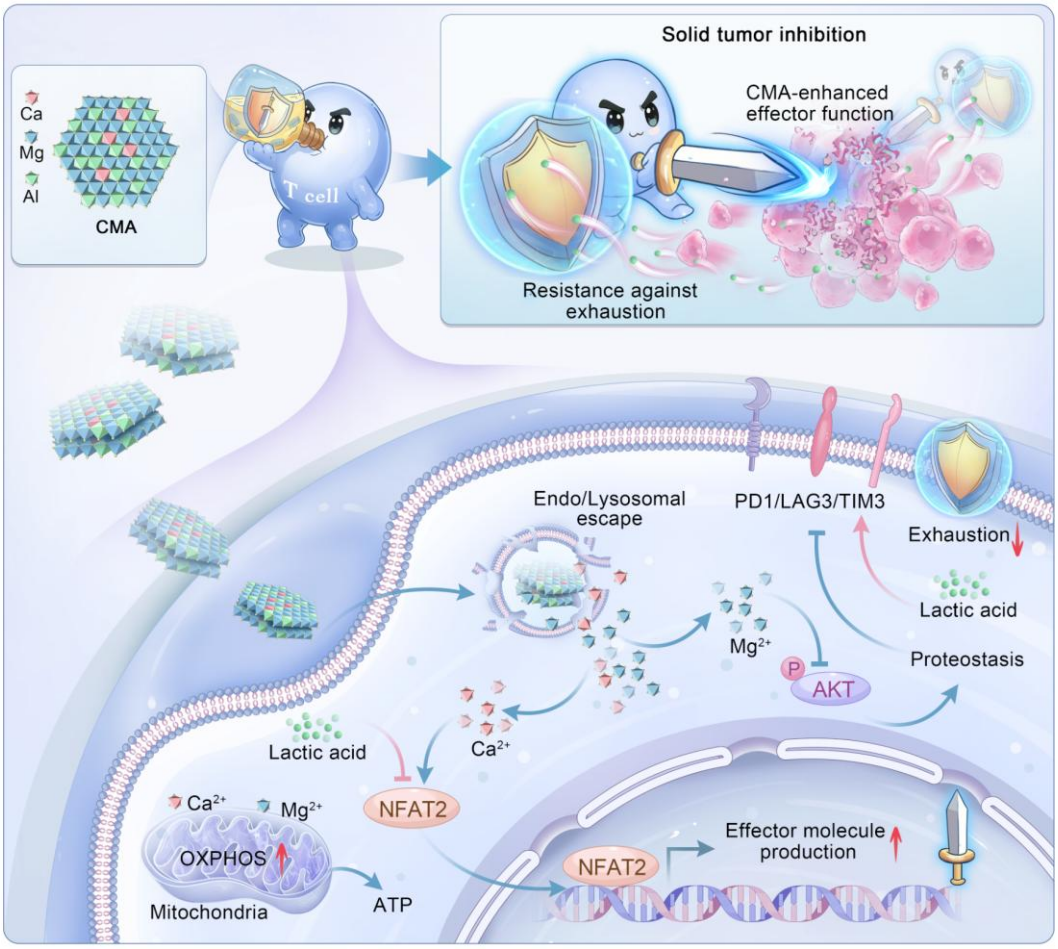

Figure 1. Schematic illustration of CMA functions as a self-braking $CD8^+$ T cell agonist promoting $CD8^+$ T cell functionality to empower cancer immunotherapy. Following internalization into $CD8^+$ T cells, CMA co-delivers Ca^{2+} and Mg^{2+} to regulate T cell function. The "sword" function is collectively

driven by Ca^{2+} and Mg^{2+} through OXPHOS enhancement, and further potentiated by Ca^{2+}-mediated NFAT2 activation to boost effector molecule production. This counteracts the suppressive effect of LA on NFAT2 signaling. The “shield” function is mediated by Mg^{2+}, which suppresses pAKT and maintains proteostasis to limit exhaustion, thereby conferring resistance against LA -induced suppression. This modulation supports both ex vivo T cell pretreatment with CMA for adoptive therapy and in situ peritumoral delivery of CMA for endogenous T cell reprogramming, culminating in potent antitumor efficacy.

2. Results and Discussion

2.1 Ca^{2+} and Mg^{2+} coordinately regulate $CD8^+$ T cell activation and exhaustion

To identify metal ion regulators capable of directly modulating $CD8^+$ T cell function, we first evaluated the effects of dietary trace elements Mg^{2+}, Ca^{2+}, Zn^{2+} and Mn^{2+} by monitoring expression of the effector cytokine interferon-γ (IFN-γ) [22]. Among these ions, Mg^{2+} and Ca^{2+} exhibited minimal cytotoxicity across the examined concentration range, whereas Zn^{2+} and Mn^{2+} induced substantial cytotoxicity at elevated concentrations (Figure 2A). Functionally, Ca^{2+} produced the strongest stimulatory effect, increasing IFN-γ expression in a concentration-dependent manner, and Mg^{2+} elicited a modest enhancement (Figure 2B). In contrast, Zn^{2+} supplementation had a limited effect on IFN-γ production, whereas Mn^{2+} reduced IFN-γ expression (Figure 2B).

To further understand the interplay between Ca^{2+} and Mg^{2+}, expression of IFN-γ and granzyme B (GzmB) was assessed in $CD8^+$ T cells cultured in either complete or Ca^{2+}-free medium. Ca^{2+} supplementation enhanced expression of both effector molecules to some extend under both conditions (Figure 2C,D). In contrast, the stimulatory effect of Mg^{2+} was observed only in the presence of extracellular Ca^{2+}, indicating that Mg^{2+}-mediated enhancement of $CD8^+$ T cell function is largely dependent on Ca^{2+}-driven activation signaling.

We next disclosed how Ca^{2+} and Mg^{2+} regulate $CD8^+$ T cell function under physiological and tumor-mimetic acidic conditions. At the physiological pH, Ca^{2+} supplementation significantly increased expression of activation markers CD69 (early stage) and CD25 (late stage) [23-24], as well as effector molecules IFN-γ and GzmB (Figure 2E). However, under LA-rich acidic conditions, which mimic the metabolic stress in the TME, activation and effector functions were markedly suppressed. Consistently, Ca^{2+} supplementation partially restored $CD8^+$ T cell activity in acidic conditions, as evidenced by increased expression of IFN-γ and GzmB (Figure 2E). In contrast, Mg^{2+} exerted limited effects on $CD8^+$ T cell activation and effector function under both conditions (Figure 2E). On the other hand, Mg^{2+} preferentially regulated T cell exhaustion while Ca^{2+} did not show any effect (Figure 2F). In particular, Mg^{2+} significantly reduced expression of the exhaustion-associated receptors programmed death 1 (PD1), lymphocyte-activation gene 3 (LAG3), and T-cell immunoglobulin and mucin-domain containing-3 (TIM3) in acidic TME-mimic medium (Figure 2F). Chronic antigen stimulation is known to induce progressive T cell exhaustion, characterized by upregulation of PD1, LAG3, and TIM3 [25]. These findings suggest that Ca^{2+} and Mg^{2+} play distinct yet complementary

roles in $CD8^+$ T cell regulation. Ca^{2+} primarily promotes activation and effector function, whereas Mg^{2+} restrains exhaustion, particularly under tumor-relevant acidic conditions. Their functional complementarity is the basis for our hypothesis that coordinated delivery of Ca^{2+} and Mg^{2+} would simultaneously enhance T cell activation but limit exhaustion, thereby generating more durable antitumor $CD8^+$ T cell responses.

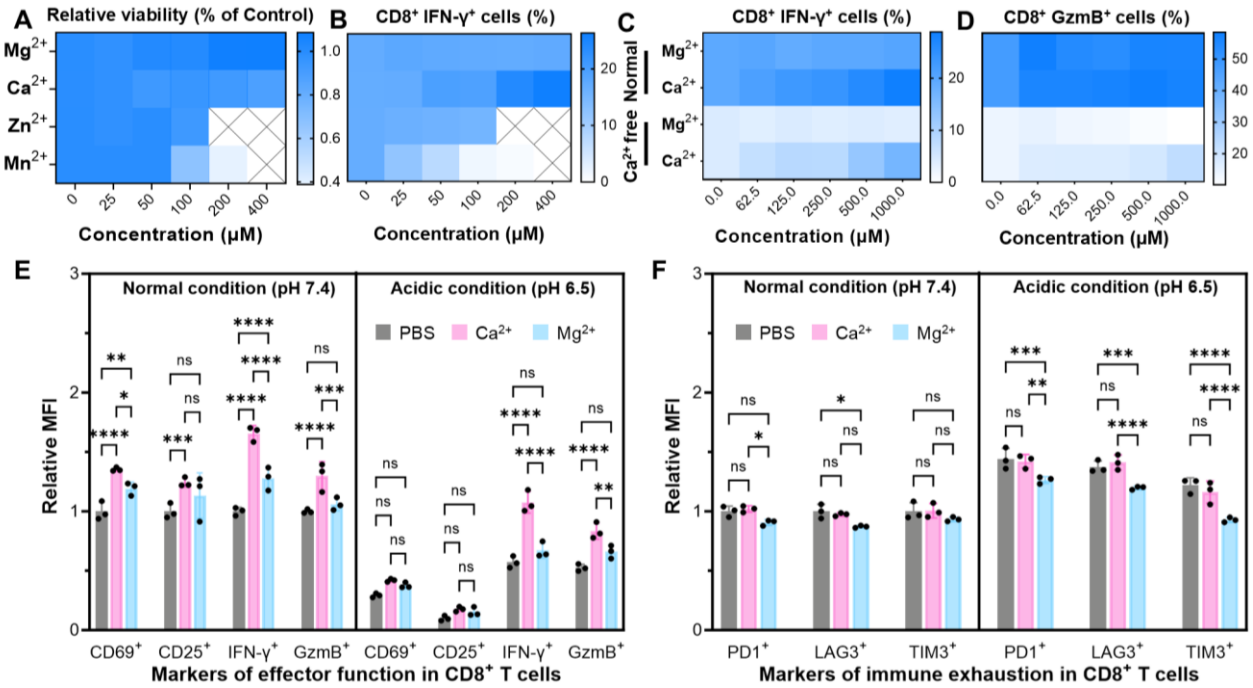

Figure 2. The immunomodulatory functions of Ca^{2+} and Mg^{2+} in $CD8^+$ T cells. Primary $CD8^+$ T cells derived from mouse spleen and lymph nodes were treated with chlorides of the indicated ions before analyzing using flow cytometry. (A, B) The relative $CD8^+$ T cells viability (A) and the expression of IFN-γ (B) in $CD8^+$ T cells treated with ions at different concentrations (the blank space denotes that the cell count is insufficient to complete a single flow cytometer assay). (C, D) $CD8^+$ T cells were culturing in Ca^{2+}-free or complete culture medium before supplementing additional Ca^{2+} and Mg^{2+} at the indicated concentrations. Then the expression of IFN-γ (C) and GzmB (D) in $CD8^+$ T cells were analyzed. (E, F) $CD8^+$ T cells were cultured in normal (pH 7.4) and acidic (pH 6.5 adjusted by LA) culture media, supplemented with additional Ca^{2+} and Mg^{2+}. Then the expression of the markers for effector function (E) and immune exhaustion (F) in $CD8^+$ T cells were analyzed. Statistical significances were computed via one-way ANOVA test. Data are shown as the mean ± s.d. (n = 3). $*p < 0.05$, $**p < 0.01$, $***p < 0.001$, $****p < 0.0001$.

2.2. Ca^{2+}-Mg^{2+} synergy enhances $CD8^+$ T cell activation while restraining exhaustion

To integrate the complementary immunoregulations of Ca^{2+} and Mg^{2+} within a single platform, Ca^{2+} was controllably incorporated into Mg^{2+}-containing MA, a layered nano-aluminum material, which was previously found to support $CD8^+$ T cell activation through neutralization of the acidic TME [15, 26]. The resulting $C_xM_{3-x}A$ formulations were prepared at the (Ca + Mg)/Al feeding molar ratio of 3:1 and x = 0.5, 1, or 2. They retained the characteristic hexagonal morphology of MA, as shown in transmission electron microscopy (TEM) images (Figure 3A). Consistently, X-ray diffraction (XRD) analysis exhibited the characteristic *(003)*, *(006)*, *(009))*, *(110)* and *(113)* reflections of the layered structure, indicating that Ca^{2+} incorporation did not interfere the crystal framework of MA (Figure 3B) [27]. Dynamic light scattering (DLS) measurements revealed comparable particle sizes among all $C_xM_{3-x}A$ formulations, whereas the zeta potential progressively decreased with increasing Ca/Mg ratio (Figure 3C and Table S1), suggesting successful incorporation of Ca^{2+} into the layered structure. Inductively coupled plasma mass spectrometry (ICP-MS) further confirmed progressive Ca^{2+} incorporation, as reflected by the increased Ca/Mg molar ratio with increasing the Ca^{2+} feed (Figure 3D and Table S1). In addition, energy-dispersive X-ray spectroscopy (EDS) mapping demonstrated homogeneous distribution of Ca^{2+}, Mg^{2+}, and Al^{3+} throughout the nanoparticles (Figure S1). Notably, increasing Ca^{2+} content also elevated the CMA suspension pH, suggesting the acid-neutralizing capacity of $C_xM_{3-x}A$ was enhanced with the incorporated Ca^{2+} amount (Figure 3E).

The release of the metal ions from C_1M_2A was found pH-dependent. Both Ca^{2+} and Mg^{2+} were largely retained within the crystal structure under physiological conditions (pH 7.4). In contrast, under TME-mimetic (pH 6.5) and endosomal-mimetic (pH 5.5) conditions, C_1M_2A exhibited distinct release kinetics for the two ions. Ca^{2+} underwent rapid release within the first 2 h, whereas Mg^{2+} was released in a more sustained manner (Figure 3F, G and Table S2). This differential release profile arises from the higher solubility of $Ca(OH)_2$ (pK_{sp} = 5.26) than $Mg(OH)_2$ (pK_{sp} = 10.74) [28]. Interestingly, the released Mg^{2+} and Ca^{2+} amount (6.8-8.7 (0.28-0.36) vs. 15.8-16.5 (0.40-0.41) μg (μmol) per mg C_1M_2A) was comparable after incubation in pH 6.5 buffers for 4-8 h.

At the cellular level, MA and $C_xM_{3-x}A$ were efficiently internalized by $CD8^+$ T cells without detectable cytotoxicity in the tested concentration range (Figure S2). Consistently with the effects of free ions, expression of activation markers CD69 and CD25 of $CD8^+$ T cells treated with MA and $C_xM_{3-x}A$ increased by 3-4 folds under both physiological and TME-mimetic conditions although their

relative levels were much lower in the latter conditions (Figure 3H and Figure S3). Similarly, production of effector molecules IFN-γ and GzmB exhibited a Ca/Mg ratio-dependent increase of 1.5-2 folds in both conditions (Figure 3H and Figure S4).

On the other hand, treatments with MA and $C_xM_{3-x}A$ all significantly reduced expression of exhaustion markers of PD1, LAG3, and TIM3 in physiological conditions by 20-30% (Figure 3I and Figure S5). In particularly, MA contained Mg^{2+} exclusively and amplified the inhibitory effect on exhaustion of free Mg^{2+} (Figure 3I, 2F), indicating that nanoparticle-mediated delivery enhanced the regulatory activity of Mg^{2+} [26]. Under TME-mimetic conditions, MA, $C_{0.5}M_{2.5}A$ and C_1M_2A treatments similarly inhibited the expression of these exhaustion markers (Figure 3I and Figure S5). However, C_2M_1A behaved very differently and did not reduce their expression (Figure 3I and Figure S5), which may be caused by the higher Ca^{2+} level delivered to T cells. A high level of Ca^{2+} ions inside effector T cells is found to inhibit early T cell activation [29]. These observations reveal that Mg^{2+} can effectively buffer Ca^{2+}-driven exhaustion within a defined compositional window (e.g. $C_{0.5}M_{2.5}A$ and C_1M_2A), thereby decoupling T cell activation from excessive exhaustion. Among the tested formulations, C_1M_2A provided the most favorable trade-off of activation, effector function, and exhaustion, and was therefore selected for subsequent studies and abbreviated as CMA.

As expected, stimulation of T cells in TME-mimetic conditions (10 mM LA, pH 6.5) led to lower activation but high exhaustion in comparison to that in physiological conditions (pH 7.4). Interestingly, C_1M_2A mostly significantly reversed these two scenarios, i.e. promoting activation and reducing exhaustion of T cells. In particular, C_1M_2A-regulated T cells in TME-mimetic conditions displayed activation and exhaustion superior or comparable to that cultured in physiological conditions, demonstrating that C_1M_2A is capable of recovering T cells impaired in TME into effector T cells normally cultured in physiological conditions.

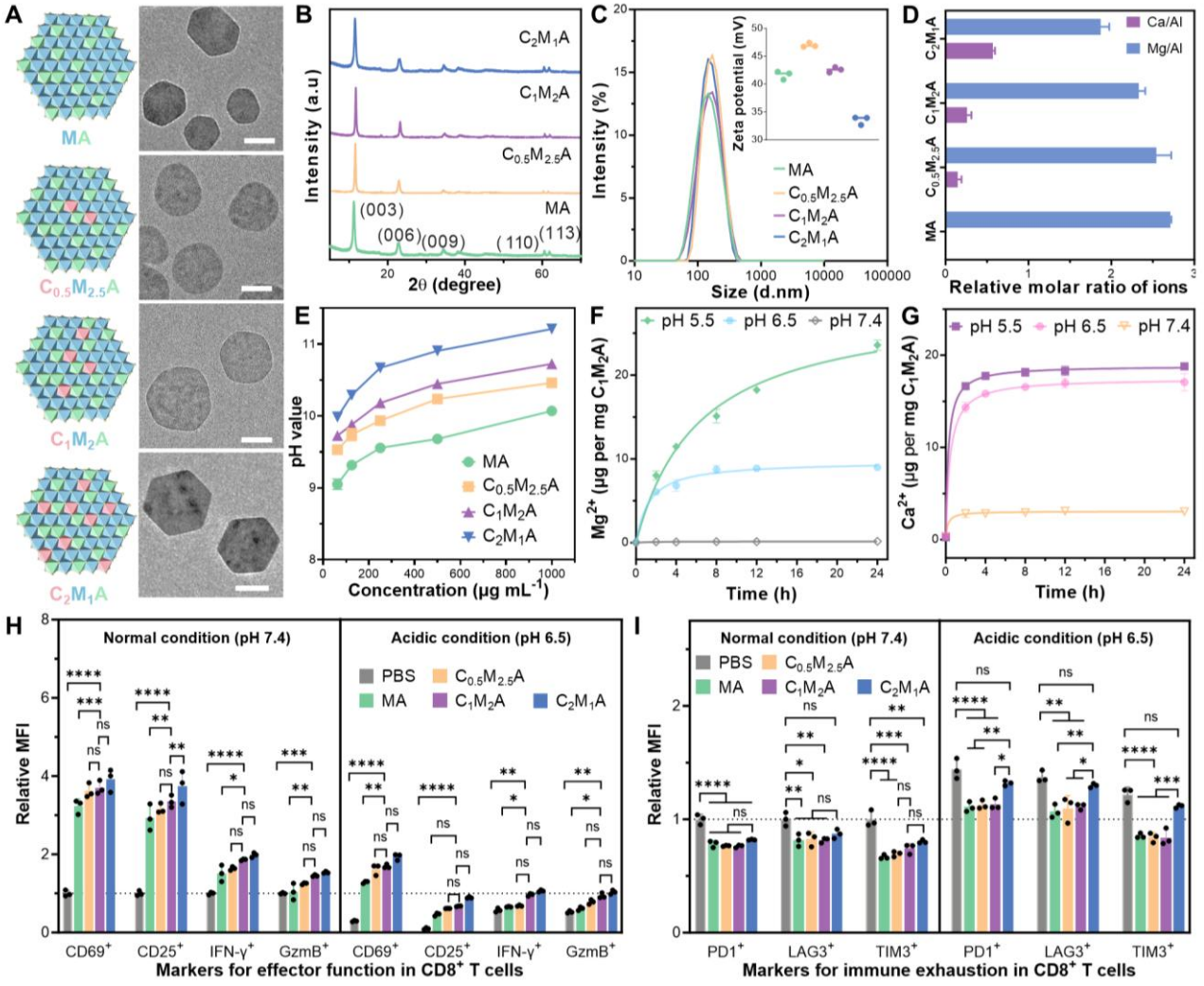

Figure 3. The immunomodulatory functions of $C_xM_{3-x}A$ in $CD8^+$ T cells. (A-E) Schematic and TEM images with scale bar of 100 nm (A), X-ray diffraction patterns (B), particle size distribution with zeta potential (C), the relative molar ratio of Ca/Al and Mg/Al (D), and solution pH (E) of MA and $C_xM_{3-x}A$. (F, G) Mg^{2+} (F) and Ca^{2+} (G) release content in different pH buffer over time. (H, I) $CD8^+$ T cells were culturing in acidic (pH 6.5 adjusted by LA) and normal (pH 7.4) culture medium before supplementing MA and $C_xM_{3-x}A$ at 100 μg mL^{-1}. Then the expression of the markers for effector function (H) and immune exhaustion (I) in $CD8^+$ T cells were analyzed. Statistical significances were computed via one-way ANOVA test. Data are shown as the mean ± s.d. (n = 3). *$p < 0.05$, **$p < 0.01$, ***$p < 0.001$, ****$p < 0.0001$.

2.3. CMA enhances $CD8^+$ T cell function through metabolic reprogramming and maintains proteostasis

We then confirmed that the superior immunomodulatory activity of CMA is associated with

metabolic reprogramming of $CD8^+$ T cells. Fluo-4-loaded $CD8^+$ T cells were stimulated with anti-CD3/CD28 for 48 h to induce T cell receptor activation [30] and subsequently treated with CMA. CMA quickly elicited a substantially greater Ca^{2+} influx than MA or the corresponding free ions, indicating more efficient intracellular Ca^{2+} mobilization under normal and acidic conditions (Figure 4A). Consistently with this enhanced Ca^{2+} influx signaling in 5 min, quantitative elemental analysis revealed significantly higher intracellular accumulation of both Mg^{2+} (12.1 ± 0.4 μg per 10^6 cells) and Ca^{2+} (1.83 ± 0.14 μg per 10^6 cells) following treatment with CMA for 24 h than the corresponding free ions (Figure 4B). Under physiological conditions, supplementation with free Ca^{2+} and Mg^{2+} modestly increased total ATP production rate in $CD8^+$ T cells (Figure S6A), and oxidative phosphorylation (OXPHOS) remained the predominant energy source (ATP rate index > 1), accompanied by moderate increases in both basal and maximal mitochondrial respiration without detectable changes in mitochondrial membrane potential (Figure S6B-D). In contrast, CMA significantly increased total ATP production, OXPHOS-dependent ATP generation, basal respiration, and maximal respiratory capacity, and these effects were more pronounced under acidic TME-mimetic conditions (Figure 4C-F).

Mechanistically, CMA markedly increased NFATc1 (NFAT2) expression compared with MA, with 53% increase under physiological conditions and 32% under LA-rich acidic conditions (Figure 4G), confirming enhanced activation of the Ca^{2+}–NFAT signaling axis [31]. In parallel, CMA reduced AKT phosphorylation to an extent comparable to MA (Figure 4H and Figure S7). NIAD-4 staining demonstrated that both CMA and MA significantly reduced protein aggregation, indicating improved proteostasis and diminished proteotoxic stress associated with T cell exhaustion (Figure 4I and Figure S8), which aligns with the established role of AKT signaling in regulating proteostasis [32]. Collectively, these findings demonstrate that CMA-mediated intracellular delivery of Ca^{2+} and Mg^{2+} coordinately remodels $CD8^+$ T cell metabolism and signaling. Rapid intracellular release of Ca^{2+} enhances mitochondrial bioenergetics and activates the Ca^{2+}–NFAT pathway to promote effector function, whereas sustained Mg^{2+} signaling suppresses AKT phosphorylation, preserves proteostasis, and limits exhaustion (Figure 4J).

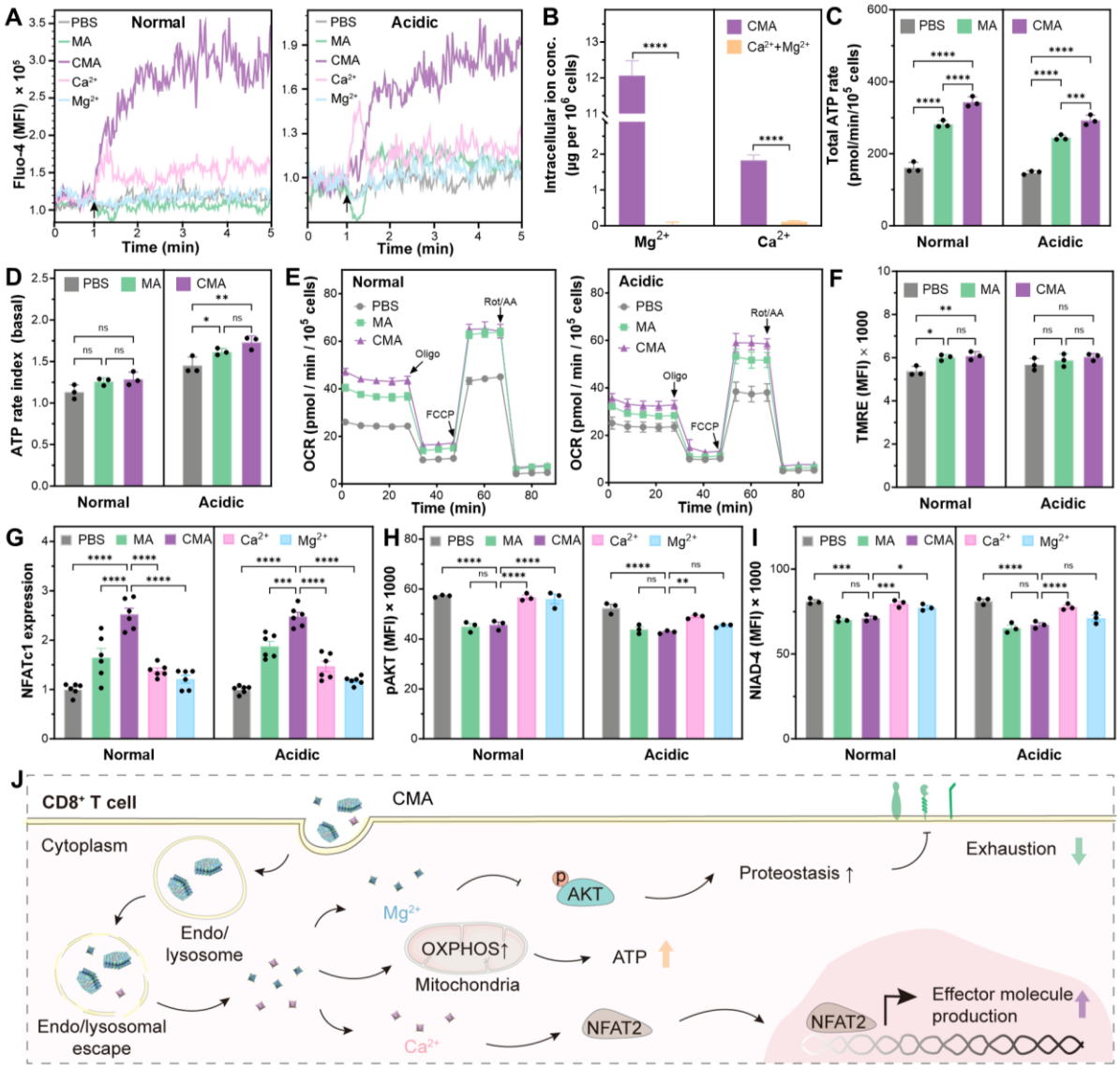

Figure 4. CMA promotes $CD8^+$ T cell metabolism and maintains proteostasis. (A) Ca^{2+} flux in $CD8^+$ T cell upon anti-CD3/CD28 stimulation and CMA treatment over 5 min under normal and acidic conditions. Black arrow marks treatment time. (B) The intracellular level of Mg^{2+} and Ca^{2+} after 24 h was assayed by ICP-MS after $CD8^+$ T cells treated with CMA (100 μg mL^{-1}). (C, D) The total basal ATP production rate (C) and ATP rate index (D) of $CD8^+$ T cell with indicated treatment. (E) Representative oxygen consumption rate (OCR) in $CD8^+$ T cells treated with CMA under normal (pH 7.4) or acidic (pH 6.5 adjusted by LA) condition. Sequential injections of oligomycin (Oligo), FCCP, and rotenone /antimycin A (Rot/AA) are indicated by black arrows. (F) Mitochondrial membrane potential (TMRE staining) in $CD8^+$ T cells treated with CMA. (G) NFATc1 expression following CMA treatment under normal (pH 7.4) or acidic (pH 6.5 adjusted by LA) condition (n = 6). (H, I) pAKT levels (H) and protein aggregation assessed by NIAD-4 staining (I) following CMA treatment. (J) Schematic illustration of the mechanism underlying CMA -mediated enhancement of $CD8^+$ T cell

function. Data are presented as the mean ± s.d. (n = 3). Statistical significance was tested by one-way ANOVA with Tukey's post hoc test. *$p < 0.05$, **$p < 0.01$, ***$p < 0.001$, ****$p < 0.0001$.

2.4. CMA pretreatment enhances effector functions and reduces exhaustion of T cells in the mimetic TME

CMA was also found to improve the cytotoxicity of adoptively transferred $CD8^+$ T cells. OT-1 $CD8^+$ T cells expressing a T cell receptor specific for the $OVA_{257-264}$ peptide (SIINFEKL) were first isolated from OT-1 mice, activated with anti-CD3/CD28 antibodies for 2 days, and used as a model of adoptive T cell therapy [33]. OT-1 cells were pretreated with CMA for 24 h and then cocultured with B16-OVA cells to assess antigen-specific cytotoxicity (Figure 5A). At an effector-to-target (E:T) ratio of 2.5:1, pretreatment with free ions or MA produced only modest improvements in tumor cell killing (18.1% for PBS versus 21.1% and 22.3%, respectively), whereas CMA significantly enhanced cytotoxicity to 29.9% (Figure 5B). A similar trend was observed at an effector-to-target ratio of 5:1, with CMA consistently outperforming both free ions and MA (Figure 5B).

Since adoptively transferred T cells rapidly encounter the metabolically hostile TME, we next showed that CMA pretreatment preserved $CD8^+$ T cell function under LA-rich acidic conditions. CMA-pretreated OT-1 cells were cultured in the TME-mimetic medium containing 5 mM LA (pH 6.8) for 24 h before functional analysis (Figure 5A). Despite acid stress, CMA-pretreated OT-1 cells maintained significantly higher expression of IFN-γ and GzmB than cells pretreated with PBS, MA, or corresponding free ions (Figure 5C,D and Figure S9A,B). In parallel, both CMA and MA reduced expression of exhaustion-associated inhibitory receptors, with CMA preserving robust effector function while limiting exhaustion (Figure 5E and Figure S9C). Under more severe acidic conditions (10 mM LA, pH 6.5), CMA continued to reduce exhaustion marker expression, but the differences were no longer statistically significant (Figure S9D). These findings indicate that CMA pretreatment enhanced the functional resilience of adoptively transferred $CD8^+$ T cells, enabling sustained effector activity under tumor-relevant metabolic stress.

We further showed that locally administered CMA regulated endogenous tumor-resident $CD8^+$ T cells similarly in vivo. Biodistribution analysis of peritumorally injected RITC-labeled CMA in B16 melanoma-bearing mice demonstrated sustained retention at the tumor site for more than 5 days, with fluorescence intensity gradually decreasing over time (Figure S10A,B). Ex vivo imaging at day 5 also

revealed preferential accumulation of CMA within tumors and tumor-draining lymph nodes, with minimal distribution to other major organs (Figure S10C,D). Histological analysis confirmed that CMA penetrated deeply into tumor tissues following peritumoral administration (Figure S10E). Consistently with the in vitro findings, peritumoral administration of CMA significantly increased the proportions of both early-activated ($CD8^+CD69^+$) and late-activated ($CD8^+CD25^+$) T cells within tumor tissues (Figure 5F and Figure S11). CMA also enhanced expression of effector molecules IFN-γ, GzmB, and TNF-α (Figure 5G,H and Figure S12), while simultaneously reducing expression of exhaustion-associated receptors PD1, LAG3, and TIM3 (Figure 5I and Figure S13). Together, these results demonstrate that CMA not only enhances the cytotoxic capacity of adoptively transferred $CD8^+$ T cells but also directly reprograms tumor-resident $CD8^+$ T cells toward a more functional, less exhausted phenotype within the immunosuppressive TME.

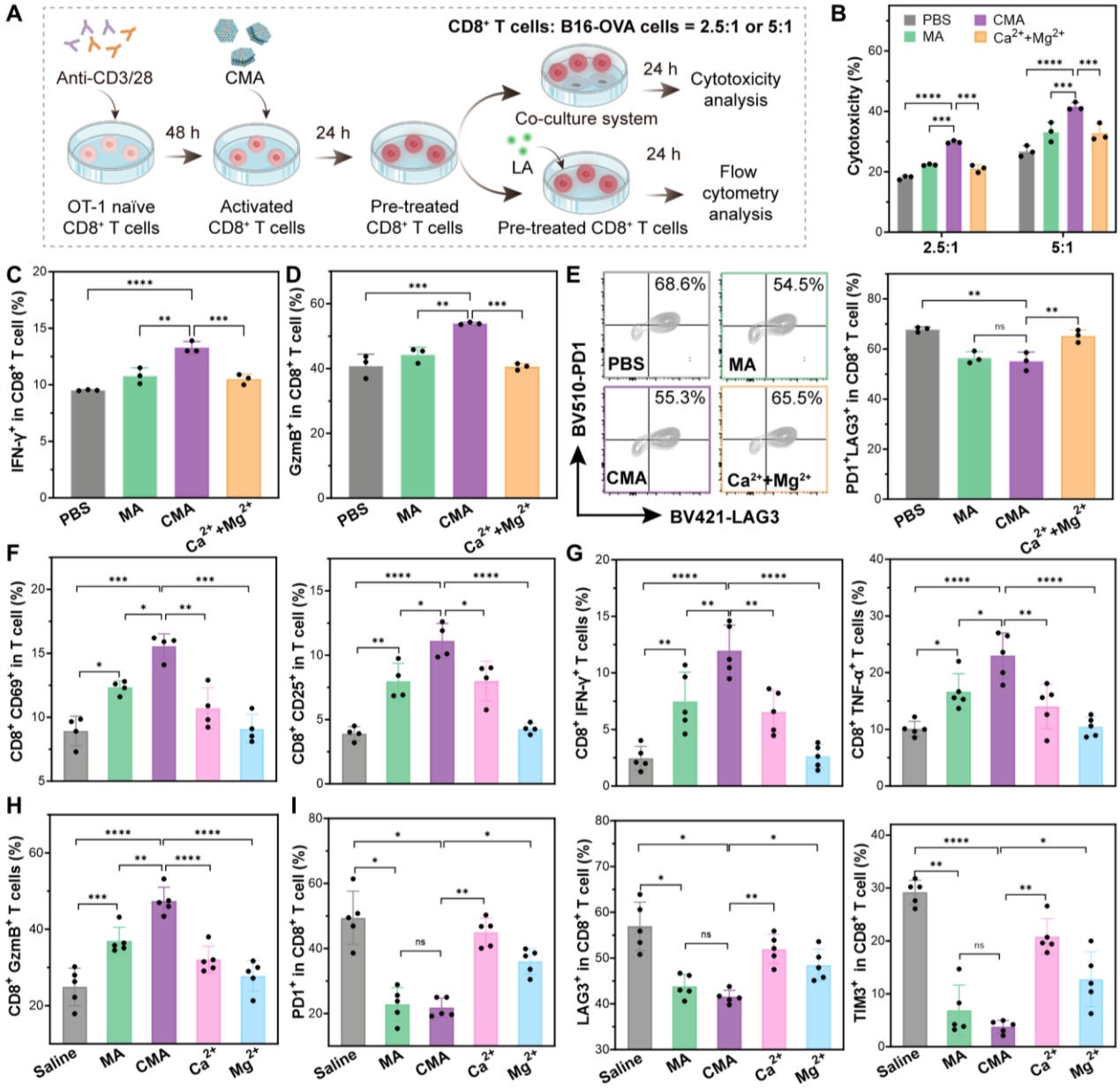

Figure 5. CMA pretreatment prevents CD8$^+$ T cell functional impairment induced by LA. (A) Schematic of CMA pretreated T cells cocultured with B16-OVA cells and challenged with LA following pretreatment with CMA. (B) Cytotoxicity mediated by pretreated T cells at E:T ratios of 2.5:1 and 5:1. (C, D) The expression of IFN-γ (C) and GzmB (D) in pretreated CD8$^+$ T cells after challenged with LA (5mM, pH = 6.8). (E) The proportion of exhausted T cells in pretreated CD8$^+$ T cells after challenged with LA (5mM, pH = 6.8). (F) Quantitative analysis of CD69 and CD25 expression in CD8$^+$ T cells within TME. (G, H) Quantitative analysis of IFN-γ, TNF-α (E) and GzmB (H) expression in CD8$^+$ T cells within TME. (I) Expression of exhaustion markers PD1, LAG3 and TIM3 in CD8$^+$ T cells within TME. Data are presented as the mean ± s.d. (n ≥ 3). Statistical significance was tested by one-way ANOVA with Tukey's post hoc test. *$p < 0.05$, **$p < 0.01$, ***p

< 0.001, ****$p < 0.0001$.

2.5. CMA enhances the antitumor efficacy of both adoptively transferred and tumor-resident CD8$^+$ T cells

CMA pretreatment seemed not to significantly alter the in vivo distribution of adoptively transferred T cells. OT-1 CD8$^+$ T cells were labeled with DiR and then retro-orbitally administered. Most transferred cells accumulated in the liver and spleen, whereas a smaller but detectable population infiltrated tumor tissues (Figure S14A-C). Peritumoral administration of CMA slightly increased tumor infiltration of adoptively transferred OT-1 cells.

The therapeutic efficacy of CMA-pretreated OT-1 cells was found to enhanced in the B16-OVA tumor model. OT-1 T cells were activated and expanded ex vivo with anti-CD3/CD28 antibodies for 2 days, followed by CMA pretreatment for an additional 24 h and adoptive transfer at day 11 and 15 after tumor inoculation (Figure 6A). Adoptive transfer of untreated OT-1 cells moderately inhibited tumor growth (21% inhibition at day 18), whereas CMA pretreatment nearly doubled the therapeutic efficacy, achieving ~38% tumor growth inhibition (Figure 6B and Figure S15). Consistently, tumor weights were significantly reduced in mice receiving CMA-pretreated OT-1 cells than in those receiving untreated OT-1 cells (Figure 6C). Immune profiling of tumor-infiltrating CD8$^+$ T cells at day 18 revealed that adoptive transfer of untreated OT-1 cells induced little change in the expression of activation (CD25) and effector molecules (IFN-γ and TNF-α), as well as exhaustion-associated receptors, compared with untreated controls (Figure 6D-H). In contrast, transfer of CMA-pretreated OT-1 cells significantly increased expression of activation and effector markers while reducing PD1, LAG3, and TIM3 expression in the overall intratumoral CD8$^+$ T-cell population (Figure 6D-H and Figure S16-17). These findings indicate that ex vivo CMA pretreatment substantially enhances the antitumor function of adoptively transferred CD8$^+$ T cells.

Since CMA also activates endogenous CD8$^+$ T cells within tumors, we further evaluated the therapeutic benefit of combining adoptively transferred CD8$^+$ T cells with local CMA administration. Peritumoral injection of CMA markedly potentiated antitumor efficacy in both treatment groups, increasing tumor growth inhibition to 68% in mice receiving untreated OT-1 cells (Figure 6B,C and Figure S15). The highly synergistic improvement is attributed to the increased number of active T cells, originating from the adoptively transferred T cells, CMA-reprogrammed tumor-resident T cells

as well as CMA-enhanced infiltrating T cells. To directly evaluate the contribution of CMA-reprogrammed tumor-resident or endogenous $CD8^+$ T cells, B16 tumor-bearing mice received peritumoral CMA at day 10 and 14 without adoptive cell transfer (Figure S18A). CMA significantly suppressed tumor growth compared with MA or free ion treatment (Figure S18B–E). Furthermore, depletion of $CD8^+$ T cells using an anti-CD8 antibody completely abolished the therapeutic efficacy of peritumoral CMA administration (Figure S19A-F), demonstrating that $CD8^+$ T cells are indispensable for CMA-mediated tumor control. Consistently with these findings, local CMA administration in combination with adoptively transferred OT-1 cells significantly increased expression of CD25, IFN-γ, GzmB, and TNF-α while reducing PD1, LAG3, and TIM3 expression in intratumoral $CD8^+$ T cells (Figure 6D-H and Figure S16-17). Furthermore, the combination of ex vivo CMA-pretreated T cells with local CMA administration achieved 89% tumor growth inhibition (Figure 6B,C and Figure S15). In line with this inhibition, intratumoral $CD8^+$ T cells in the combination group showed elevated expression of CD25, IFN-γ, GzmB, and TNF-α, along with reduced PD1, LAG3, and TIM3 levels even compared with the CMA+OT-1 group (Figure 6D-H and Figure S16-17).

In addition, CMA exhibited a favorable safety profile. Body weights of mice remained stable throughout treatment, with no significant differences among control and experimental groups (Figure S20). Hematological analysis showed no detectable alterations in red blood cell, white blood cell, or platelet counts at the experimental endpoint (Figure S21A), and histological examination revealed no apparent pathological abnormalities in major organs (Figure S21B). Collectively, these results demonstrate that CMA safely enhances the antitumor activity of both adoptively transferred and endogenous tumor-resident $CD8^+$ T cells, resulting in superior control of solid tumor growth.

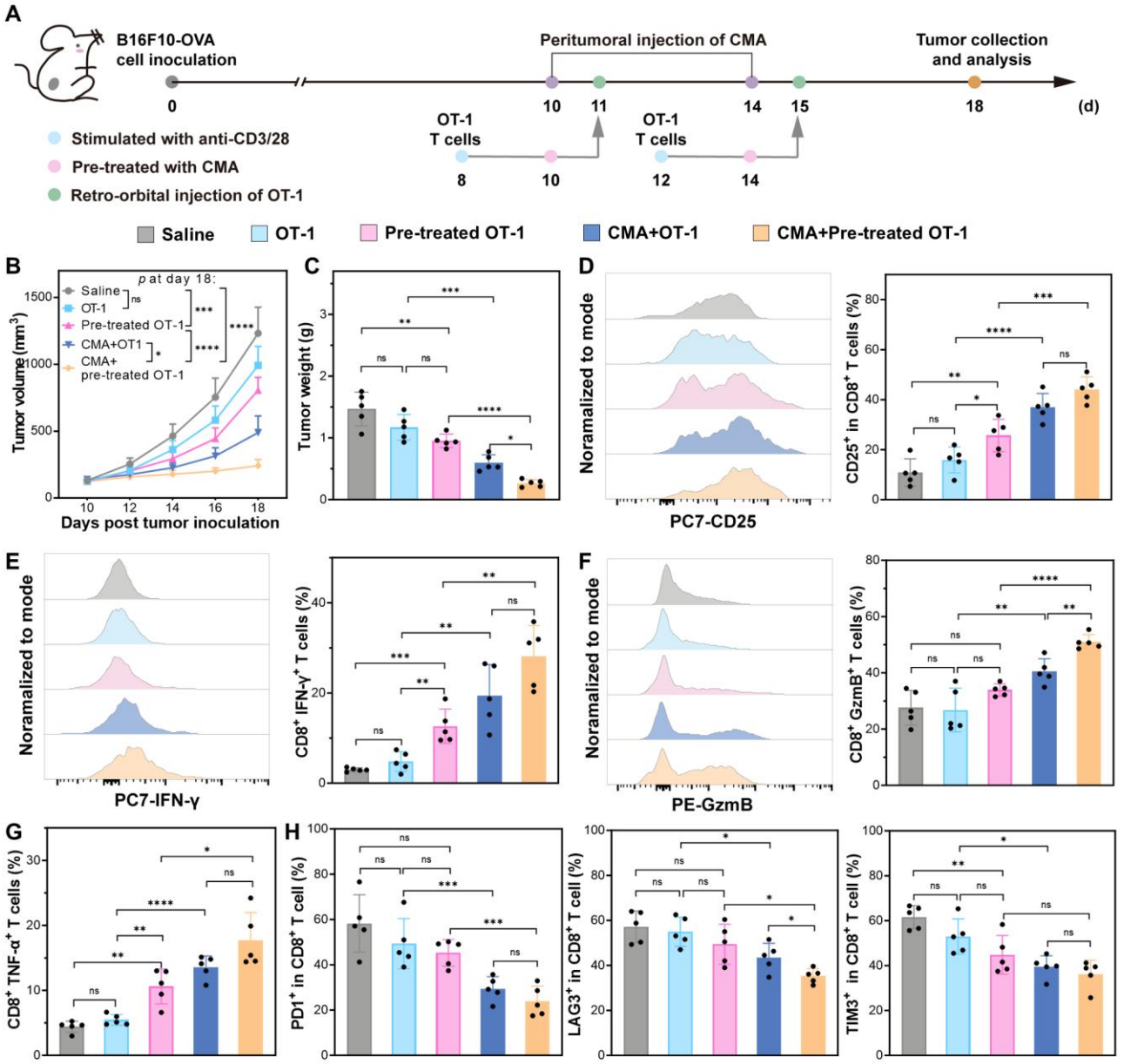

Figure 6. CMA pretreatment empowers OT-1 $CD8^+$ T cell and promotes adoptive cell therapy. (A) Schematic illustration of the treatment timeline in the B16-OVA melanoma model. (B) Mean tumor growth curves over time. (C) Tumor weights measured at day 18. (D-F) Representative flow cytometry histograms and quantitative analysis of CD25 (D), IFN-γ (E) and GzmB (F) expression in $CD8^+$ T cells within TME. (G) TNF-α expression in $CD8^+$ T cells within TME following indicated treatments. (H) Expression of exhaustion markers PD1, LAG3 and TIM3 in $CD8^+$ T cells within TME. Data are presented as the mean ± s.d. (n = 5). Statistical significance was tested by unpaired t test. *$p < 0.05$, **$p < 0.01$, ***$p < 0.001$, ****$p < 0.0001$.

3. Conclusion

$CD8^+$ T cells are key to antitumor immunity, but their function is often compromised by the hostile TME. Given the critical role of Ca^{2+} and Mg^{2+} on $CD8^+$ T cell function, we reasoned that co-delivery of these two ions could preserve $CD8^+$ T cell function in the TME. Thus, we developed a dual-metal-ion $CD8^+$ T cell agonist, CMA, that simultaneously enhances $CD8^+$ T cell effector function and attenuates exhaustion under both physiological and TME-mimicking conditions. Notably, CMA pretreatment endows $CD8^+$ T cells with intrinsic resistance to LA-mediated suppression, demonstrating the capacity of CMA to pre-empower T cells against the acidic TME. CMA pretreatment of $CD8^+$ T cells markedly enhanced the therapeutic efficacy of adoptive T cell therapy. In addition, peritumoral administration of CMA alone significantly suppressed B16 melanoma growth. Consistently, the combination of CMA-pretreated $CD8^+$ T cells with peritumoral CMA injection further potentiated the antitumor efficacy of adoptive T cell therapy.

Mechanistically, internalized CMA released Ca^{2+} ions to promote OXPHOS and activate NFAT2 signaling to boost effector molecule production, while inhibiting pAKT to maintain proteostasis and limit exhaustion via released Mg^{2+}. The enhanced activation was accompanied by a moderate upregulation of exhaustion-associated inhibitory receptors. However, the co-delivery of Ca^{2+} and Mg^{2+} at a proper ratio uncoupled this association, providing sufficient Ca^{2+} to drive effector function without escalating exhaustion, due to the counterbalancing effect of Mg^{2+} on proteostatic regulation. Notably, CMA regulates T cell activation and exhaustion of $CD8^+$ T cells under TME-mimetic condition, bringing their functional status to a level comparable to that of normal conditions.

To our knowledge, this is the first demonstration that optimally calibrates $CD8^+$ T cell effector function and exhaustion through Ca^{2+}/Mg^{2+} regulation. Furthermore, we introduce a non-genetic, ex vivo priming strategy using CMA to confer LA resistance on $CD8^+$ T cells. Moreover, CMA is a bifunctional adjuvant that both primes T cells ex vivo for adoptive cell therapy and preserves $CD8^+$ T cell function in situ via peritumoral injection. However, the precise molecular mechanism by which Mg^{2+} enhances OXPHOS and suppresses pAKT remains incompletely defined, and whether these findings extend to other cancer types (e.g., breast, lung) remains to be determined. Future work should evaluate CMA in additional tumor models. In summary, CMA offers a simple and versatile immune agonist that functions both as an ex vivo T cell priming platform and as a local $CD8^+$ T cell enhancer agent, representing a promising strategy to improve cancer immunotherapy.

4. Materials and Methods

Materials and Reagents. $CaCl_2{\cdot}2H_2O$, $MgCl_2{\cdot}6H_2O$, $AlCl_3{\cdot}9H_2O$, and NaOH were purchased from Aladdin (China). Fluorescein 5-isothiocyanate (FITC) was purchased from MedChemExpress (USA). Antibodies and dyes used for flow cytometry (Table S3) were obtained from BioLegend (USA), BD Bioscience (USA), Abcam (UK), Invitrogen (USA) or MedChemExpress (USA).

Cell Lines and Animals. B16F10, B16F10-OVA, and B16F10-Luc cell lines (American Type Culture Collection, ATCC) were maintained in RPMI 1640 supplemented with fetal bovine serum (FBS) and penicillin-streptomycin. $CD8^+$ T cells were enriched from spleens and lymph nodes of wild-type C57BL/6 or OT-1 transgenic mice using the MojoSort™ Mouse CD8 T Cell Isolation Kit (#480035, Biolegend, USA). T cells were cultured in RPMI 1640 containing FBS, antibiotics, 2-mercaptoethanol, L-glutamine, and sodium pyruvate.

Animal studies were approved by the Animal Care and Use Committee of Shenzhen Bay Laboratory (approval No. AEXZP202302). Female C57BL/6 mice (6-8 weeks) were obtained from Gempharmatech (China) and housed under specific pathogen-free conditions. OT-1 mice (C57BL/6-Tg(TcraTcrb)1100Mjb/J) were purchased from Geneandpeace (China).

Preparation and Characterization of $C_xM_{3-x}A$. A mixed salt solution (10 mL) containing $CaCl_2{\cdot}2H_2O$ (0, 0.05, 0.10, or 0.20 mol L^{-1}) $MgCl_2{\cdot}6H_2O$ (0.3, 0.25, 0.20, or 0.10 mol L^{-1}) and $AlCl_3{\cdot}9H_2O$ (0.10 mol L^{-1}) was rapidly added to NaOH solution (0.2 mol L^{-1}, 40 mL) under vigorous stirring for 30 min. Then collected precipitate was washed twice, and resuspended in 40 mL of deionized water. For the synthesis of $C_{0.5}M_{2.5}A$ and C_1M_2A, the suspensions were hydrothermally treated at 100 °C for 16 h. For the synthesis of MA and C_2M_1A, the suspensions were sequentially treated at 100 °C for 6 h and then at 150 °C for 6 h.

Morphological features of $C_xM_{3-x}A$ were examined with TEM (Talos L120C G2, Thermo Fisher, USA). Elemental composition and distribution were analyzed via EDS (JEM-F200, JEOL, Japan) and ICP-MS (Agilent, USA). Crystal structure was determined via XRD patterns (SmartLab, Rigaku Corporation, Japan), while particle size distribution and zeta potential were assessed using DLS (Zetasizer Pro, Malvern Panalytical, England).

Cellular Uptake and Cell Cytotoxicity. $CD8^+$ T cells were incubated with FITC- labelled $C_xM_{3-x}A$ (100 μg mL^{-1}) for 24 h, after which the percentage of positive cells was assessed via flow cytometry. Separately, cells were stained with Fixable Viability Stain 700 (564997, BD Biosciences, USA) for cell viability assessment via flow cytometry.

Ion Release and Cellular Uptake Profiles of CMA. CMA (100 μg mL^{-1}) was incubated in buffers at varying pH (5.5, 6.5, or 7.4) over time, and released Ca^{2+} and Mg^{2+} in the supernatant were quantified by ICP-MS. For cellular uptake, $CD8^+$ T cells were incubated with CMA for 24 h, and the intracellular Ca^{2+} and Mg^{2+} levels were detected by ICP-MS.

Flow Cytometry Analysis of $CD8^+$ T Cell Function in vitro. For assessment of $CD8^+$ T cell activation, naïve $CD8^+$ T cells were first activated in medium containing anti-CD3/CD28 for 48 h under LA (10 mM) or normal conditions, followed by staining with anti-CD69 and anti-CD25 antibodies and analysis using flow cytometry (CytoFLEX LX, Beckman Coulter, USA). For evaluation of effector function and exhaustion, activated $CD8^+$ T cells were incubated with PBS, MA, CMA, Ca^{2+} or Mg^{2+} for 24 h under LA (10 mM) or normal conditions, followed by staining with antibodies against IFN-γ, GzmB, PD1, LAG3 and TIM3, and analyzed using flow cytometry (CytoFLEX LX, Beckman Coulter, USA; Aurora, Cytek, USA). To determine whether pretreatment rescues $CD8^+$ T cell effector function and attenuates exhaustion under LA stress, cells were pretreated with PBS, MA, CMA, or Ca^{2+}+Mg^{2+} for 24 h, then cultured in medium containing LA (5 or 10 mM) for an additional 24 h. Cells were subsequently stained with the same antibody panel and analyzed using flow cytometry.

Separately, activated T cells were treated with various nutritional metal ions (Mg^{2+}, Ca^{2+}, Zn^{2+}, Mn^{2+}, and Co^{2+}) at indicated concentrations, after which relative cell viability and IFN-γ expression were assessed by flow cytometry. In another parallel experiment, activated T cells were treated with Ca^{2+} or Mg^{2+} in Ca^{2+}-free medium, and the proportions of IFN-γ and granzyme B positive cells were determined using flow cytometry.

Metabolism Analysis by Seahorse. Activated $CD8^+$ T cells were incubated with Saline, MA, CMA, Ca^{2+} or Mg^{2+} for 24 h under LA (10 mM) or normal conditions. The cells were then seeded in poly-D-lysine coated XF96 microplates at a density of 2×10^5 cells per well. For real-time ATP production

rate assay (Seahorse XF Real-Time ATP Rate Assay Kit, #103592-100, Agilent, USA), the hydrated sensor cartridge was loaded with oligomycin (1 μM) and Antimycin-A/Rotenone (Rot/AA, 0.5 μM), followed by analysis in the XF96 Analyzer. For OCR assessment (Seahorse XF Cell Mito Stress Test Kit, #103015-100, Agilent, USA), the sensor cartridge was sequentially loaded with oligomycin (1 μM), FCCP (2.5 μM) and Rot/AA (0.5 μM), and analyzed using the same instrument.

Mitochondrial Membrane Potential and Cellular Proteostasis Analysis. Activated $CD8^+$ T cells were treated with PBS, MA, CMA, Ca^{2+} or Mg^{2+} for 24 h. For the mitochondrial membrane potential assessment, the cells were stained with TMRE (100 nM) at 37 ℃ for 15 min and analyzed using flow cytometry (CytoFLEX LX, Beckman Coulter, USA). For the cellular proteostasis evaluation, treated cells were fixed and then permeabilized using True-Phos^{TM} Perm Buffer (#76344, BioLegend, USA), followed by staining with anti-pAKT antibody for 30 min. In a parallel experiment, cells were stained with NIAD-4 (100 nM) at 37 ℃ for 30 min to assess protein aggregation.

Ca^{2+} Influx Measurement. Naïve $CD8^+$ T cells were first loaded with Fluo-4-AM (2 μM). After recording baseline fluorescence for 1 min, anti-CD3/CD28 together with PBS, MA, CMA, Ca^{2+} or Mg^{2+} was added, and Ca^{2+} flux was measured via flow cytometry for another 4 min.

Quantitative Real-Time PCR Analysis of NFAT2 Expression. Activated $CD8^+$ T cells were treated with PBS, MA, CMA, Ca^{2+} or Mg^{2+} for 24 h, then the total RNA was extracted using the Steady Pure Universal RNA Extraction Kit II (#AG21022, Vazyme, China) and reverse transcription was performed with the Hifair® III 1st Strand cDNA Synthesis SuperMix (#11141ES10, Vazyme, China). NFAT2 expression was quantified with real-time PCR using SYBR Green (#11201ES08, Yeasen, China) with the following primers: forward, 5'-CGCACGCCTTCTACCAAGTA-3'; reverse, 5'-GTCGATGGTGGCTCTCATGT-3'. GAPDH was used as an internal control with primers: forward, 5'-AAATGGTGAAGGTCGGTGTGAAC-3'; reverse, 5'-CAACAATCTCCACTTTGCCA CTG-3'.

Cell Killing Assay. Activated OT-1 $CD8^+$ T cells were pretreated with PBS, MA, CMA, or Ca^{2+}+Mg^{2+} for 24 h, then co-cultured with B16-OVA cells for additional 24 h at the effector to target ratio of

2.5:1 and 5:1. The supernatant was collected, and lactate dehydrogenase release was measured using a commercial kit (#C0017, Beyotime, China), with the absorbance read at 490 nm and 680 nm on a microplate reader (H1, Agilent, USA).

Biodistribution of CMA or OT-1 CD8$^+$ T Cells in vivo. For CMA biodistribution, RITC- labeled CMA was injected peritumorally into B16 melanoma-bearing mice, and fluorescence intensity was monitored over time using an in vivo imaging system (IVIS Spectrum, PerkinElmer, USA). After 5 days, major organs and tumors were harvested and imaged ex vivo. Tumor sections were further examined using slide scanner (VS200, Evident, Japan).

For OT-1 CD8$^+$ T cell biodistribution, DiR-labeled T cells were administered retro-orbitally into B16-OVA melanoma-bearing mice with or without CMA co-administration. After 4 days, major organs and tumors were collected for fluorescence intensity analysis (IVIS Spectrum, PerkinElmer, USA).

Antitumor Efficacy in vivo. B16-OVA cells (5×10^5 cells /mouse) were inoculated into female C57BL/6 mice (6-8 weeks). When tumors reached ~ 120 mm^3, CMA was injected peritumorally at day 10 and 14. Activated OT-1 CD8$^+$ T cells were pretreated with CMA for 1 day. The pretreated OT-1 T cells were administered retro-orbitally at day 11 and 15. Tumor volumes and body weights were recorded every two days, and tumor weights were measured at day 18.

Separately, B16 cells (5×10^5 cells / mouse) were inoculated into female C57BL/6 mice (6-8 weeks). When tumors reached ~ 100 mm^3, CMA was injected peritumorally at day 10 and 14. Tumor volumes were monitored every two days.

CD8$^+$ T Cell Depletion in vivo. To deplete CD8$^+$ T cells, B16 melanoma-bearing mice received intraperitoneal injections of anti-CD8 antibody (150 μg per mouse) at day 10 and 14. CMA was administered peritumorally on the same days. Tumor volumes were monitored every two days. At day 18, tumors were harvested, and tumor sections were stained with FITC-conjugated anti-CD8 antibody and scanned using a slide scanner (VS200, Evident, Japan). Peripheral blood was collected and stained with antibodies against CD45, CD3, CD4, and CD8, followed by flow cytometric analysis (CytoFLEX LX, Beckman Coulter, USA).

Analysis of $CD8^+$ T cell Function ex vivo. Harvested tumors were dissociated into single-cell suspensions using the Tumor Dissociation Kit (#130-096-630, Miltenyi, Germany). Cells were stained with antibodies against CD69, CD25, IFN-γ, GzmB, TNF-α, PD1, LAG3 and TIM3, and analyzed via flow cytometry (CytoFLEX LX, Beckman Coulter, USA; Aurora, Cytek, USA).

Statistical Analysis. Data are presented as the mean ± s.d. ($n \geq 3$). Statistical significance was tested by one-way ANOVA with Tukey's post hoc test. $*p < 0.05$, $**p < 0.01$, $***p < 0.001$, $****p < 0.0001$. Analyses were performed using GraphPad Prism.

Acknowledgements

The authors acknowledged Shenzhen Bay Laboratory startup grant awarded to Professor Z.P. Xu, Shenzhen Bay Laboratory Fenji Postdoctoral Project and Shenzhen City Postdoctoral Fund to Dr. J Zhao.

References

1. C. Scirgolea, R. Sottile, M. De Luca, et al., "Nacl Enhances Cd8+ T Cell Effector Functions in Cancer Immunotherapy," *Nature Immunology* 25, no. 10 (2024), https://doi.org/10.1038/s41590-024-01923-9.

2. M.T. Lotze, S.H. Olejniczak, and D. Skokos, "Cd28 Co-Stimulation: Novel Insights and Applications in Cancer Immunotherapy," *Nature Reviews Immunology* 24, no. 12 (2024), https://doi.org/10.1038/s41577-024-01061-1.

3. Z.L. Lamplugh, N. Wellhausen, C.H. June, and Y. Fan, "Microenvironmental Regulation of Solid Tumour Resistance to Car T Cell Therapy," *Nature Reviews Immunology* 26, no. 3 (2026), https://doi.org/10.1038/s41577-025-01229-3.

4. H. Abken, "Car T Cell Therapies in Gastrointestinal Cancers: Current Clinical Trials and Strategies to Overcome Challenges," *Nature Reviews Gastroenterology & Hepatology* 22, no. 7 (2025), https://doi.org/10.1038/s41575-025-01062-y.

5. U. Uslu, and C.H. June, "Beyond the Blood: Expanding Car T Cell Therapy to Solid Tumors," *Nature Biotechnology* 43, no. 4 (2025), https://doi.org/10.1038/s41587-024-02446-2.

6. Y. Wu, Y. Wu, Z. Gao, W. Yu, L. Zhang, and F. Zhou, "Revitalizing T Cells: Breakthroughs and Challenges in Overcoming T Cell Exhaustion," *Signal Transduction and Targeted Therapy* 11, no. 1 (2026), https://doi.org/10.1038/s41392-025-02327-3.

7. M.-Q. Yang, S.-L. Zhang, L. Sun, et al., "Targeting Mitochondria: Restoring the Antitumor Efficacy of Exhausted T Cells," *Molecular Cancer* 23, no. 1 (2024), https://doi.org/10.1186/s12943-024-02175-9.

8. Y. Liu, A.S. Sperling, E.L. Smith, and D.J. Mooney, "Optimizing the Manufacturing and Antitumour Response of Car t Therapy," *Nature Reviews Bioengineering* 1, no. 4 (2023), https://doi.org/10.1038/s44222-023-00031-x.

9. P. Ginefra, H. Carrasco Hope, M. Spagna, A. Zecchillo, and N. Vannini, "Ionic Regulation of T-Cell

Function and Anti-Tumour Immunity," *International Journal of Molecular Sciences* 22, no. 24 (2021).

10. R. Eil, S.K. Vodnala, D. Clever, et al., "Ionic Immune Suppression within the Tumour Microenvironment Limits T Cell Effector Function," *Nature* 537, no. 7621 (2016), https://doi.org/10.1038/nature19364.

11. J. Ma, L. Tang, Y. Tan, et al., "Lithium Carbonate Revitalizes Tumor-Reactive Cd8+ T Cells by Shunting Lactic Acid into Mitochondria," *Nature Immunology* 25, no. 3 (2024), https://doi.org/10.1038/s41590-023-01738-0.

12. W. Yang, Z. Feng, X. Lai, et al., "Calcium Nanoparticles Target and Activate T Cells to Enhance Anti-Tumor Function," *Nature Communications* 15, no. 1 (2024), https://doi.org/10.1038/s41467-024-54402-y.

13. K.-D. Kim, S. Bae, T. Capece, et al., "Targeted Calcium Influx Boosts Cytotoxic T Lymphocyte Function in the Tumour Microenvironment," *Nature Communications* 8, no. 1 (2017), https://doi.org/10.1038/ncomms15365.

14. A. Baessler, and D.A.A. Vignali, "T Cell Exhaustion," *Annual Review of Immunology* 42, no. Volume 42, 2024 (2024), https://doi.org/https://doi.org/10.1146/annurev-immunol-090222-110914.

15. A. Shen, J. Zhao, Z. Su, et al., "Interleukin 12-Tethered Nano-Aluminum Adjuvant Orchestrates Environmental Immunomodulation to Empower Cytotoxic T Cells against Solid Tumors," *Acta Pharmaceutica Sinica B* (2025), https://doi.org/https://doi.org/10.1016/j.apsb.2025.10.021.

16. J. Lötscher, I.L.A.A. Martí, N. Kirchhammer, et al., "Magnesium Sensing Via Lfa-1 Regulates Cd8(+) T cell Effector Function," *Cell* 185, no. 4 (2022), https://doi.org/10.1016/j.cell.2021.12.039.

17. C. Kanellopoulou, A.B. George, E. Masutani, et al., "Mg2+ Regulation of Kinase Signaling and Immune Function," *Journal of Experimental Medicine* 216, no. 8 (2019), https://doi.org/10.1084/jem.20181970.

18. T. Hu, Z. Gu, G.R. Williams, et al., "Layered Double Hydroxide-Based Nanomaterials for Biomedical Applications," *Chemical Society Reviews* 51, no. 14 (2022), https://doi.org/10.1039/D2CS00236A.

19. L. Zhang, Y. Jia, J. Yang, et al., "Efficient Immunotherapy of Drug-Free Layered Double Hydroxide Nanoparticles Via Neutralizing Excess Acid and Blocking Tumor Cell Autophagy," *ACS Nano* 16, no. 8 (2022), https://doi.org/10.1021/acsnano.2c02183.

20. B. Li, Y. Tan, J.H. Lei, et al., "Alkaline Adjuvant Regulates Proteolytic Activity of Macrophages for Antigen Cross-Presentation and Potentiates Radioimmunotherapy," *Advanced Materials* 37, no. 12 (2025), https://doi.org/https://doi.org/10.1002/adma.202416690.

21. L. Zhang, J. Zhao, X. Hu, et al., "A Peritumorally Injected Immunomodulating Adjuvant Elicits Robust and Safe Metalloimmunotherapy against Solid Tumors," *Advanced materials (Deerfield Beach, Fla.)* 34, no. 41 (2022), https://doi.org/10.1002/adma.202206915.

22. R. Thibaut, P. Bost, I. Milo, et al., "Bystander Ifn-Γ Activity Promotes Widespread and Sustained Cytokine Signaling Altering the Tumor Microenvironment," *Nature Cancer* 1, no. 3 (2020), https://doi.org/10.1038/s43018-020-0038-2.

23. A. Ray, M. Bassette, K.H. Hu, et al., "Multimodal Delineation of a Layer of Effector Function among Exhausted Cd8 T Cells in Tumors," *Science Immunology* 10, no. 109 (2025), https://doi.org/doi:10.1126/sciimmunol.adt3537.

24. K. Starska, E. Głowacka, A. Kulig, I. Lewy-Trenda, M. Bryś, and P. Lewkowicz, "The Role of Tumor Cells in the Modification of T Lymphocytes Activity--the Expression of the Early Cd69+, Cd71+ and the Late Cd25+, Cd26+, Hla/Dr+ Activation Markers on T Cd4+ and Cd8+ Cells in Squamous Cell Laryngeal Carcinoma. Part I," *Folia Histochem Cytobiol* 49, no. 4 (2011).

25. Y. Huang, A. Jia, Y. Wang, and G. Liu, "Cd8(+) T Cell Exhaustion in Anti-Tumour Immunity: The New Insights for Cancer Immunotherapy," *Immunology* 168, no. 1 (2023), https://doi.org/10.1111/imm.13588.

26. Y. Jia, J. Hu, C. Zhu, et al., "Engineered Nanoalum from Aluminum Turns Cold Tumor Hot for Potentiating Cancer Metalloimmunotherapy," *Journal of Controlled Release* 354(2023), https://doi.org/10.1016/j.jconrel.2023.01.043.

27. J. Zhao, L. Zhang, P. Li, et al., "An Immunomodulatory Zinc-Alum/Ovalbumin Nanovaccine Boosts Cancer Metalloimmunotherapy through Erythrocyte-Assisted Cascade Immune Activation," *Adv Sci (Weinh)* 11, no. 6 (2024), https://doi.org/10.1002/advs.202307389.

28. N. Sun, J. Jing, H. Jiang, et al., "Effects of Surfactants and Alkalis on the Stability of Heavy-Oil-in-Water Emulsions," *SPE Journal* 22, no. 01 (2016), https://doi.org/10.2118/181742-pa.

29. P. Sharma, A. Guo, S. Poudel, et al., "Early Methionine Availability Attenuates T Cell Exhaustion," *Nature Immunology* 26, no. 8 (2025), https://doi.org/10.1038/s41590-025-02223-6.

30. I. Hamaidi, P. Cheng, S.Y. Jun, et al., "Sirt2-Mediated Deacetylation of Lck Governs the Magnitude of T Cell Receptor Signaling," *Nature Immunology* 27, no. 2 (2026), https://doi.org/10.1038/s41590-025-02377-3.

31. S. Klein-Hessling, K. Muhammad, M. Klein, et al., "Nfatc1 Controls the Cytotoxicity of Cd8+ T Cells," *Nature Communications* 8, no. 1 (2017), https://doi.org/10.1038/s41467-017-00612-6.

32. Y. Wang, A. Ma, N.-J. Song, et al., "Proteotoxic Stress Response Drives T Cell Exhaustion and Immune Evasion," *Nature* 647, no. 8091 (2025), https://doi.org/10.1038/s41586-025-09539-1.

33. C. Zhu, C. Liu, Q. Wu, et al., "Remolding the Tumor Microenvironment by Bacteria Augments Adoptive T Cell Therapy in Advanced-Stage Solid Tumors," *Signal Transduct Target Ther* 9, no. 1 (2024), https://doi.org/10.1038/s41392-024-02028-3.